### **Action: respond to our copy-editing questions**

Select each question and describe any changes we should make on the proof. Changes against journal style will not be made and proofs will not be sent back for further editing.

- AQ1: Please check all author names and affiliations. Please check that author surnames have been identified by a pink background. This is to ensure that forenames and surnames have been correctly tagged for online indexing.
- AQ2: If your manuscript has figures or text from other sources, please ensure you have permission from the copyright holder. For any questions about permissions contact jnls.author.support@oup.com.
- AQ3: Please check that funding is recorded in a separate funding section if applicable. Use the full official names of any funding bodies, and include any grant numbers.
- AQ4: You may need to include a "conflict of interest" section. This would cover any situations that might raise any questions of bias in your work and in your article's conclusions, implications, or opinions. Please see here.
- AQ5: Please ensure that you provide the city, postal code and country for the affiliations.
- AQ6: Please check the changes made in the sentence 'Depending on a variety of parameters, such as the age...' and correct if necessary.
- AQ7: Please spell out NSF in the text.
- AQ8: Please check if Bao et al. (2021) has been published. If it has been, kindly update the reference.
- AQ9: Please provide the publisher location for Evensen (2006), Murray (2007) and Segel (1984).

These proofs are for checking purposes only. They are not in final publication format. Please do not distribute them in print or online. Do not publish this article, or any excerpts from it, anywhere else until the final version has been published with OUP. For further information, see https://academic.oup.com/journals/pages/authors

Figure resolution may be reduced in PDF proofs and in the online PDF, to manage the size of the file. Full-resolution figures will be used for print publication.

## Action: check your manuscript information

Please check that the information in the table is correct. We use this information in the online version of your article and for sharing with third party indexing sites, where applicable.

Full affiliations Each unique affiliation should be listed separately; affiliations must contain only the applicable department, institution, city, territory, and country.  Group contributors	1 Department of Mathematics, Florida State University, 208 Love Building, Tallahassee, Fl 32306 2 Dr. Phillip Frost Department of Dermatology and Cutaneous Surgery, University of Miami Miller School of Medicine, Miami, FL, USA, Centre for Dermatology Research, University of Manchester, and NIHR Biomedical Research Centre, Manchester, UK 3 School of Mathematical and Natural Sciences, Arizona State University, West Campus, and Department of Mathematics, North Carolina State University NA
The name of the group and individuals in this group should be given, if applicable (e.g. The BFG Working Group: Simon Mason, Jane Bloggs)	
Supplementary data files cited	NA
Funder Name(s) Please give the full name of the main funding body/agency. This should be the full name of the funding body without abbreviation or translation, if unsure, see https://search.crossref.org/funding	National Science Foundation NIHR Manchester Biomedical Research Centre NSF

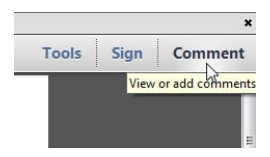
### How to add your responses

These instructions show you how to add your responses to your proof using Adobe Acrobat Professional version 7 onwards, or Adobe Reader DC. To check what version you are using, go to 'Help', then 'About'. The latest version of Adobe Reader is available for free from <a href="https://get.adobe.com/uk/reader/">https://get.adobe.com/uk/reader/</a>.

#### Displaying the toolbars

#### **Adobe Reader DC**

In Adobe Reader DC, the Comment toolbar can be found by clicking 'Comment' in the menu on the top-right-hand side of the page (shown below).

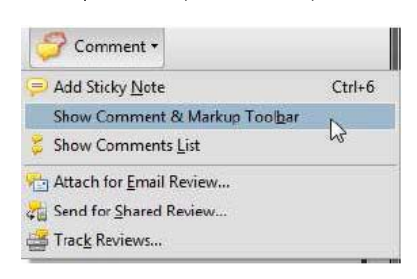


The toolbar shown below will then display along the right-hand-side of the page.



#### Acrobat Professional 7, 8 and 9

In Adobe Professional, the Comment toolbar can be found by clicking 'Comment(s)' in the top toolbar, and then clicking 'Show Comment & Markup Toolbar' (shown below).



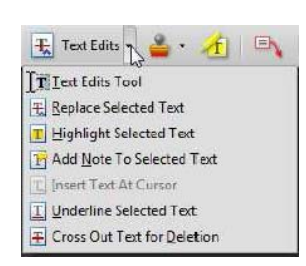
The toolbar shown below will then be displayed along the top of the page.



#### Using text edits and comments in Acrobat

This is the easiest method to both make changes, and for your changes to be transferred and checked.

- 1. Click 'Text Edits'
- 2. Select the text to be annotated or place your cursor at the insertion point and start typing.
- 3. Click the 'Text Edits' drop down arrow and select the required action.
- You can also right click on selected text for a range of commenting options, or to add sticky notes.



#### Using commenting tools in Adobe Reader

All commenting tools are displayed in the toolbar. You cannot use text edits, however you can still use highlighter, sticky notes, and a variety of insert/replace text options.



#### Pop-up notes

In both Reader and Acrobat, when you insert or edit text, a pop-up box will appear.

#### **Saving comments**

In order to save your comments and notes, you need to save the file ('File', 'Save') before closing the document.

NB: Do not make any edits directly into the text, use commenting tools only

*Mathematical Medicine and Biology: A Journal of the IMA* (2021) **00**, 1–19 doi:10.1093/imammb/dqab008

# Data assimilation of synthetic data as a novel strategy for predicting disease progression in alopecia areata

N.G. COGAN\* AND FENG BAO

Department of Mathematics, Florida State University, 208 Love Building, Tallahassee, Fl 32306

RALF PAUS

Dr. Phillip Frost Department of Dermatology and Cutaneous Surgery, University of Miami Miller School of Medicine, Miami, FL, USA, Centre for Dermatology Research, University of Manchester, and NIHR Biomedical Research Centre, Manchester, UK

AND

#### Atanaska Dobreva

School of Mathematical and Natural Sciences, Arizona State University, West Campus, and
Department of Mathematics, North Carolina State University

\*Corresponding author: cogan@math.fsu.edu

[Received on 30 April 2020; revised on 27 April 2021; accepted on 6 May 2021]

The goal of patient-specific treatment of diseases requires a connection between clinical observations with models that are able to accurately predict the disease progression. Even when realistic models are available, it is very difficult to parameterize them and often parameter estimates that are made using early time course data prove to be highly inaccurate. Inaccuracies can cause different predictions, especially when the progression depends sensitively on the parameters. In this study, we apply a Bayesian data assimilation method, where the data are incorporated sequentially, to a model of the autoimmune disease alopecia areata that is characterized by distinct spatial patterns of hair loss. Using synthetic data as simulated clinical observations, we show that our method is relatively robust with respect to variations in parameter estimates. Moreover, we compare convergence rates for parameters with different sensitivities, varying observational times and varying levels of noise. We find that this method works better for sparse observations, sensitive parameters and noisy observations. Taken together, we find that our data assimilation, in conjunction with our biologically inspired model, provides directions for individualized diagnosis and treatments.

Keywords: personalized medicine; data assimilation; autoimmunity; alopecia areata.

#### 1. Author summary

Overall goals for personalized medicine include adjusting disease treatments for individual patients and based on observations obtained during the disease progression and treatment. This requires predictive models that can rapidly be tuned to specific patients during the course of disease and treatment regimen. One of the difficulties is that many models use parameters that are not directly measurable and must be estimated. Moreover, observations are typically incomplete and do not provide estimates of all variables in a mathematical model. In this study, we describe how to assimilate partial observations using a recently developed direct filter data assimilation (Bao *et al.*, 2021, 2019). We use synthetic data to show how this method can be used to overcome difficulties that are specific to biological models

AQ5

including parameters that are sensitive to measurements, noisy and incomplete data and data that may

# be sporadically observed, longitudinally.

#### 2. Introduction/background

2

Alopecia areata (AA) is the most common, chronic inflammatory human hair loss disease. It affects all age groups and types of hair follicles (HFs) (e.g. scalp, facial, etc.) as well as both genders. With few exceptions (i.e. diffuse AA), this disease shows a pathognomonic hair loss pattern that is characterized by progressive patches of hair loss in seemingly normal, visibly non-inflamed skin, the presence of broken-off or tapered hair shafts ('cadaver hairs', 'exclamation mark hairs') and/or the regrowth of white hair shafts within an alopecic lesion (Gilhar *et al.*, 2012). Depending on a variety of parameters, such as the age of first AA onset, the presence of associated autoimmune diseases, atopy or Down syndrome, or a positive family history for AA, there is tremendous variation in patient prognosis (Gilhar *et al.*, 2012; Strazzulla *et al.*, 2018).

Clinicians managing patients with AA face several vexing problems. There are few satisfactory treatments available and the response of AA patients to any kind of therapy is linked to their relative prognosis. There are no reliable methods to predict how fast AA lesions will progress in this specific patient, and how he/she will respond to therapy (Gilhar *et al.*, 2012). With the recent introduction of JAK inhibitors (Wang *et al.*, 2018; Phan & Sebaratnam, 2019), this therapeutic dilemma has improved greatly. However, there is still a need for a tool to classify the state of the disease within a patient.

Given these challenges in the management of AA, it would be of substantial clinical and pharmacological interest to develop a mathematical method for predicting how fast and extensively the hair loss lesions seen in a given patient will expand and coalesce over time and/or will be replaced by active hair regrowth. This would finally empower physicians to inform and educate their AA patients regarding their individual hair loss and disease prognosis. Additionally, such a predictive model would be most welcome for calculating whether a rather mild AA therapy (e.g. relatively safe and inexpensive topical glucocorticosteroids) will likely suffice for halting hair loss progression and for promoting hair regrowth in a given patient or whether it is advisable to opt for a more aggressive form of therapy (e.g. systemic JAK inhibitor) in a patient with a poor prognosis and high likelihood of rapid disease progression. Theoretically, such a model could then replace the rough empirical prognostic estimates that physicians have to rely on today.

Systematically building upon our previous modelling approaches to AA (Dobreva *et al.*, 2020, 2015, 2017), the current study explores and proposes a pathway to achieve exactly this. We first review pertinent biological hypotheses that form the basis for our model formulation. We then describe the model, mainly to provide context for the presentation of the assimilation method and to keep this manuscript self-contained. We then describe the data assimilation method used here followed by detailed numerical exploration/prediction examples.

#### 2.1 Biological hypotheses

Alopecia is a cell-mediated autoimmune disease of the HF, which results from an interferon-gamma (IFNg)-driven attack of CD8+ T lymphocytes on growing (anagen) HFs that have lost their unique immuno-inhibitory milieu ('immune privilege collapse'). The HFs then present HF-derived autoantigens via MHC class Ia molecules to autoreactive CD8+ T cells (Gilhar *et al.*, 2012; Paus *et al.*, 2006). In recent years, it has become increasingly understood that innate immunocytes, such as natural killer cells (Gilhar *et al.*, 2013; Ito *et al.*, 2008; Petukhova *et al.*, 2010) and mast cells (Bertolini *et al.*, 2014),

AQ6

also play an important role in the immune pathogenesis of AA. Autoantigen-independent pathological activities of these cells can also suffice to induce the clinical hair loss phenomena (Pratt *et al.*, 2017). Moreover, it is appreciated that AA occurs in distinct sub-types, which may reflect differences in AA pathogenesis (Gilhar *et al.*, 2012; Ikeda, 1965).

All this has invited the concept that AA does not necessarily and always represent a classical autoimmune disease, but primarily is a stereotypic response pattern of otherwise healthy anagen HFs that (a) have lost their immune privilege (for various reasons) and (b) become the target of an IFNg-dominated immunocyte attack. This then leads to HF damage (HF dystrophy), abrupt termination of anagen (i.e. premature catagen development) and thus hair shaft shedding and ultimately alopecia with typical patterned hair loss (Solomon, 2015). In some AA patients, this can indeed result from a classical, HF autoantigen- and CD8+ T cell-dependent autoimmune response. Yet in other patients, the characteristic AA type of hair loss may result from pathogenic activities of innate immunocytes that secrete excessive amounts of IFNg, which alone suffice to induce all hallmarks of AA, i.e. immune privilege collapse, HF dystrophy and premature catagen induction, but fail to meet the criteria of a classical autoimmune disease. Thus, AA is not necessarily a disease but always a distinct response pattern of the HF to immunological damage (Solomon, 2015).

#### 2.2 Mathematical background

Previously, we used ordinary differential equations (ODEs) and partial differential equations (PDEs) to model the development of AA. Our ODE models describe the temporal immune attack dynamics in anagen HFs (Dobreva *et al.*, 2015) and cycling HFs (Dobreva *et al.*, 2017) and capture states of health, disease and treatment. In alignment with the medical consideration that AA is driven by sufficient clonal expansion and aggregation of immunocytes in HFs (Gilhar *et al.*, 2012), our findings reveal that HFs in anagen become diseased if the populations of immune cells launching the attack, orchestrated by IFNg, grow significantly large (Dobreva *et al.*, 2015). In the model where we incorporated HF cycling (Dobreva *et al.*, 2017), our components for immune players interact with equations for the human hair cycle (Al-Nuaimi *et al.*, 2012). This enhanced ODE system enabled us to accurately show that in response to the immunological insult against hair-producing cells, the process of hair growth is abruptly stopped, and the regression phase catagen is prematurely induced (Dobreva *et al.*, 2017).

Our PDE model for AA is 1D and reflects the changes in time and in space of the key immune components involved in the disease development, IFNg (*IFN*), CD8<sup>+</sup> T-cells (*T*8) and CD4<sup>+</sup> T-cells (*T*4). The dynamics of IFNg consist of production by T-cells ( $p_{IFN}(T4+T8)$ ), degradation ( $-\delta_{IFN}IFN$ ) and diffusion ( $D_{IFN}\Delta IFN$ ). IFNg activates CD8<sup>+</sup> T-cells  $\left(\frac{\alpha IFN}{1+s}\right)$  and CD4<sup>+</sup> T-cells  $\left(\frac{\beta IFN}{1+s}\right)$ . The CD4<sup>+</sup> T-cell population expands and helps CD8<sup>+</sup> T-cells to proliferate  $\left(\frac{p_T\gamma T4T8}{1+s}\right)$ .

The lymphocyte activation and clonal expansion are inhibited by immuno-supressive substances produced in the HF environment, called immune privilege guardians. This inhibitory effect on the immune cell dynamics is captured through the parameter s. Rather than posit specific mechanisms, we treat the immune privilege as a parameter. This is consistent with the immune privilege guardian hypotheses (Gilhar et al., 2012; Ito et al., 2008) and allows us to investigate the consequence of the state of the guardianship, potentially providing clinically verifiable insight.

Both immunocyte populations experience natural  $(-\delta_T T8)$ ,  $(-\delta_T T4)$  and concentration-dependent  $(-\kappa_T (T8)^2)$ ,  $(-\kappa_T (T4)^2)$  cell death. Also, they move randomly  $(D_{T8}\Delta T8)$ ,  $(D_{T4}\Delta T4)$  and exhibit chemotactic movement up the concentration gradient in IFNg  $(-\chi \nabla \cdot (T8\nabla IFN))$ ,  $(-\chi \nabla \cdot (T4\nabla IFN))$ .

Table 1	Base	parameters	used in	this	manuscript
---------	------	------------	---------	------	------------

Parameter	Meaning	Value
$p_{IFN}$	IFN production	$0.115 \ pg \ day^{-1}$
$p_T$	T-cell production	$0.004 \ day^{-1}$
$D_{IFN}$	Diffusion rate of IFN	$10^{-2} cm^2 day^{-1}$
$D_{T4}$ and $D_{T8}$	Diffusion rate of T4 and T8	$10^{-3} cm^2 day^{-1}$
$\delta_{IFN}$	Decay rate of IFN	$1day^{-1}$
$\delta_{T4}$ and $\delta_{T8}$	Death rate of T4 and T8	$0.05 day^{-1}$
γ	Recruitment rate of T4 <sup>+</sup> and T8 <sup>+</sup>	$0.08pg^{-1}$
α	Recruitment rate of T8 <sup>+</sup>	$0.8975pg^{-1}$
χ	Signalling sensitivity	$10^{-6} cm^2 day^{-1}$
S	Immune guardian suppression	0.01(dimensionless)

The model equations are given below, and the parameter values, listed in Table 1, are as discussed in our previous study (Dobreva *et al.*, 2020).

$$\begin{split} \frac{\partial IFN}{\partial t} &= p_{IFN}(T4+T8) - \delta_{IFN}IFN + D_{IFN}\Delta IFN \\ \frac{\partial T8}{\partial t} &= \frac{\alpha IFN}{1+s} + \frac{p_T\gamma T4T8}{1+s} - \delta_T T8 - \kappa_T T8^2 \\ &- \chi \nabla \cdot (T8\nabla IFN) + D_{T8}\Delta T8 \end{split} \tag{2}$$

$$\frac{\partial T4}{\partial t} &= \frac{\beta IFN}{1+s} + \frac{p_T T4}{1+s} - \delta_T T4 - \kappa_T T4^2 \\ &- \chi \nabla \cdot (T4\nabla IFN) + D_{T4}\Delta T4. \tag{3}$$

The boundary conditions are assumed to be periodic with the scale of the domain set by the disease progression (Dobreva *et al.*, 2020). In this manuscript, we restrict the model to one spatial dimension; however, the methods are readily extendible to higher dimensions.

The PDE model successfully captures the distinct disease patterns in agreement with experimental findings. These patterns are linked to the underlying spatio-temporal dynamics of immune cells and signals involved in the disease development (Dobreva *et al.*, 2020). The results indicate that hairless lesions are areas where HF immune privilege collapse is induced by sufficiently elevated IFNg, and the accumulation of activated immunocytes has become large enough to inflict damage on hair-producing cells. Thus, the disease state observed by hairless patches is determined by distinct regions of elevated immunocytes. We also explored how different processes reflected in the model impact pattern emergence and analysed the pattern propagation in a larger domain (Dobreva *et al.*, 2020). Throughout this manuscript, we use parameters determined in Dobreva *et al.* (2020) as our nominal set (see Table 1).

#### 2.3 Current study

One of the difficulties in AA is the varied response to treatment and difficulty in classifying the disease state. How can we use clinical observations to guide treatment, given this variability? It is essentially impossible to observe or measure the components that are required to understand the details of the

disease—namely components of the immune system (e.g. CD4<sup>+</sup> and CD8<sup>+</sup> T-cells). Instead, patches can be measured and the progression of the patches of hair loss can be followed. In this study, we are interested in using this partial data to provide more precise predictions of the disease course. Using our previously developed model (Dobreva *et al.*, 2020), we can predict the rate of spread of the pattern—as long as we know the parameters. Therefore, it is crucial to be able to estimate the parameters accurately using partial observations. Parameter estimates can also be coupled with sensitivity analysis that was previously performed to provide a window into treatment and care plans that are individualized and based on patient observations. Thus, we account for variations both within the patient populations and within a single patient through the course of the disease and treatment. By combining robust methods for estimating the parameters and a model that reflects the current understanding of the disease, we are able to determine estimates of the parameters—and hence classify the disease state and progression. The parameter estimate is shown to be reasonably accurate with respect to variations in parameters and positive convergence characteristics with respect to parameter sensitivity, observational frequency and observational noise.

There are several issues that must be overcome. This is an example of the classical 'what they measure, we cannot predict and what we can predict, they cannot measure' puzzle that confronts the intersection of theory and applications. In this case, the reduced model that we have developed includes compartments for one signalling cytokine, interferon  $\gamma$  and two components of the active immune system, CD4<sup>+</sup> and CD8<sup>+</sup> T-cells. The disease presentation in our model is implicitly treated as a threshold in state variables—i.e. we connect the hair-loss patterns directly with the predicted values of the immune cells.

The timescale of the disease course also presents a challenge. Typical observations are separated by several months and it is not clear whether more observations are required, and if so, on what timescale. Therefore, one goal of this study is to determine the timing of observations that allows for the most accurate and quickest estimation of the parameters, which in turn describes the state of the disease. A second goal is to determine what effect noise has on the rate of convergence of parameter estimates since the measurements that we are using may be inaccurate. Finally, we consider the convergence in terms of observations, both length of observational time and the gap between observations.

We use a relatively new tool for parameter estimation to obtain biologically, and potentially clinically, relevant conclusions for our biologically rooted model. While this is still closer to the theoretical realm (since the data have not been collected and we are using synthetic data), the methods used and results obtained indicate a very robust method that has direct impact on experimental design and potential clinical treatment.

#### 3. Data assimilation

The goal of data assimilation is to estimate the state of some stochastic system based on observational data. In most situations, the data we collect provide only partial information of the state and are perturbed by some noise. Popular methods for data assimilation include Kalman type filters (Del Moral et al., 2018; Evensen, 2006, 2009; Tong et al., 2016), particle filters (Andrieu et al., 2010; Gordon et al., 1993; Kang et al., 2018; Pitt & Shephard, 1999; Morzfeld et al., 2012; van Leeuwen, 2010) and probability density approximation based methods (Bao & Maroulas, 2017; Bao et al., 2021, 2019; Zakai, 1969). Although in many situations data assimilation methods are used to estimate hidden states of dynamical systems, in practice, data assimilation is also a powerful tool to estimate parameters that govern dynamical models.

6

In this approach, we design a computational framework to estimate the unknown parameters in the AA model (1)–(3) by collecting clinical data from patients as noisy observation to formulate a data assimilation problem. Specifically, we assume that we can observe features that reflect solutions  $T_4$  and  $T_8$  of the (1)–(3), and we design observations  $\{Y_4^i\}$  and  $\{Y_8^j\}$  defined by

$$Y_4^i(t) := T_4(x_i, t) + \epsilon_t^i,$$

$$Y_8^j(t) := T_8(x_i, t) + \epsilon_t^j,$$
(4)

where  $\epsilon_t$  is time-space noise and  $\{x_i\}$ ,  $\{x_j\}$  are grid points used to discretize equations for  $T_4$  and  $T_8$ . Although it is difficult to directly observe the levels of immune components, the model developed above follows the hypothesis of a direct connection between high levels of immune cells and disease symptoms of hair loss.

Let  $\theta$  be the vector representing the unknown parameters, we aim to find  $E[\theta|\mathcal{Y}_{0:t}]$  as the best estimate for the quantity of interest (QOI), i.e.  $\theta$ , where  $\mathcal{Y}_{0,t} := \sigma(T_4^i(s) \vee T_8^j(s), 0 \le s \le t)$  is the  $\sigma$ -algebra generated by  $\{Y_4^i\}$  and  $\{Y_8^j\}$  containing all the observational information. We do not provide synthetic data for IFN, we first approximate solution at the current parameter estimates to (2) and use this to complete the observational information (e.g. incomplete observations).

We first briefly discuss the general framework of data assimilation, which is usually given by the following state-space model of a nonlinear dynamical system

$$S_{n+1} = F(S_n) + \xi_n,$$
  

$$O_{n+1} = G(S_{n+1}) + \zeta_{n+1},$$
(5)

where  $n \geq 0$  is a time series,  $\{\xi_n\}$  and  $\{\zeta_n\}$  are two sequences of random variables representing noise that perturbs the system and people typically assume that  $\xi_n$  and  $\zeta_n$  are typically assumed to be Gaussian variables. The stochastic process  $\{S_n\}$  is called the 'state process', which describes the state of some mathematical model F with uncertainty  $\xi$  involved in the model. The process  $\{O_n\}$  gives the noisy partial observations for the state  $S_n$  through the observation function G, which is called the 'observation process'. The goal of the data assimilation is to obtain the best estimate for the state  $S_n$  given the observation process  $\{O_n\}$ . Mathematically, we need to find the *optimal filter* for  $S_n$ , denoted by  $\tilde{S}_n$  with

$$\tilde{S}_n := E[S_n | O_{1:n}],$$

where  $O_{1:n} := \sigma(O_1, O_2, \dots, O_n)$ .

We formulate the parameter estimation problem that we aim to solve as a data assimilation problem as first described in Archibald *et al.* (2019). That is, we use the dynamical system defined in (5) and then solve the parameter estimation problem using a Bayesian framework. We introduce a time-space partition  $\mathcal{T} \times \Pi_M$  for the PDE system (1)–(3), where  $\mathcal{T} := \{t_0 < t_1 < t_2, \ldots\}$  is a progressive temporal partition set with  $t_0 = 0$ ;  $\Pi_M := \{x_i : a = x_0 < x_1 < x_2 < \cdots < x_M = b\}$  is the spatial partition and we let a (or b) be the lower (or upper) boundary of the spatial domain. Over the partition  $\mathcal{T} \times \Pi_M$ , we write the numerical scheme for solving the PDE system as

$$X_{n+1} = \Phi(X_n, \lambda, \theta), \tag{6}$$

where the vector  $X_n := (I\hat{F}N, \hat{T}_4, \hat{T}_8)$  represents our approximate solution for IFN,  $T_4$  and  $T_8$  in the AA model (1)–(3) on all the spatial points in  $\Pi$  at time instant  $t_n$  and  $\Phi$  denotes the numerical approximation operator that maps  $X_n$  to  $X_{n+1}$  with a given set of parameters  $\lambda$  that we already know and the choice of unknown parameter vector  $\theta$  that we need to estimate. The observations that we collect to help us estimate  $\theta$  are the data from (4), which are received in the discrete form as follows:

$$Y_{n+1} = H(X_{n+1}) + \epsilon_{n+1} \tag{7}$$

where  $H(X_{n+1}) = (T_4, T_8)$  gives the observations for  $T_4$  and  $T_8$  and  $\epsilon_{n+1}$  is the noise that perturbs the observations. In this way, we actually have  $Y_{n+1} = (Y_4, Y_8)$  for  $Y_4$  and  $Y_8$  defined in (4). With the dynamical system (6)–(7), the parameter estimation problem that we are interested in this work is to get the best estimate of  $\theta$  given the observations  $Y_{1\cdot n}$ , i.e. find  $\tilde{\theta} = E[\theta|Y_{1\cdot n}]$ .

We introduce the following pseudo parameter process

$$\theta_{n+1} = \theta_n + \eta_n,\tag{8}$$

where  $\eta_n$  is an artificial dynamic noise and  $\theta_0$  is the initial guess of the parameter in the model. Then, the goal of parameter estimation becomes to obtain a dynamical estimate  $\tilde{\theta}_n := E[\theta_n | Y_{1:n}]$ , where  $Y_n$  is the observation introduced in (7). In the direct filter, we modify the observation  $Y_n$  to incorporate the model information contained in the PDE solver  $\Phi$ . Specifically, we let

$$Y_{n+1} = H(\Phi(X_n, \lambda, \theta_{n+1})) + \epsilon_{n+1},$$

where we have represented  $X_{n+1}$  by  $\Phi(X_n, \lambda, \theta_{n+1})$  which is derived from (6) by using  $\theta_{n+1}$  to replace  $\theta$ . In this way, the above observation process contains both the observation information and the model dynamics. To create a stronger connection between the model and observation, we use the observation  $Y_n$  as our approximation for  $T_4$  and  $T_8$  in the state vector  $X_n$  and write  $\tilde{X}_n = (I\hat{F}N, Y_4, Y_8)$ , where  $Y_4$  and  $Y_8$  are introduced in (4). In this way, we have the following modified observation process:

$$\tilde{Y}_{n+1} = H(\Phi(\tilde{X}_n, \lambda, \theta_{n+1})) + \epsilon_{n+1}. \tag{9}$$

As a result, we obtain a data assimilation problem by combining (8) and (9). The optimal filter we obtain in this way is now  $E[\theta_n|\tilde{Y}_{1:n}]$ . For the specific numerical implementation to obtain the optimal filtering that solves the data assimilation problem (8)–(9), we refer to Archibald *et al.* (2019).

#### 4. DA: numerical experiments guided by previous model analysis and clinical needs

In this section, we present numerical experiments to demonstrate the performance of the parameter estimation methodology that we introduced in this paper for the AA model in the online manner. Recall that we identify patterns of hair loss from high levels of immune cells that are predicted by our model. Since the parameters themselves are uncertain and are the goal of the DA, it is important to understand the interaction between sensitivity and estimation. It is typical to argue that sensitive parameters are the most crucial to estimate since they have the largest effect on the output. Intuition might argue that these would be the most difficult to estimate; however, we show below that this is not the case. In fact, sensitivity enhances the convergence of the method.

7

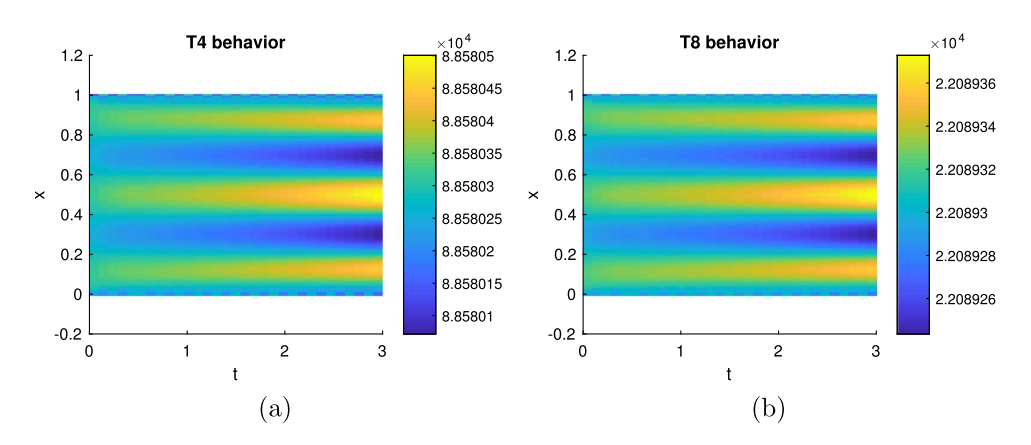


Fig. 1. Using our nominal (e.g. 'true') parameters, we simulate the development of the spatial pattern obtained from numerical simulations of (1)–(3). Parameter values are given in Table 1. (a) Simulated solution T4. (b) Simulated solution T8.

We also consider two situations guided by clinical restrictions. First, because the observations are difficult to perform in the clinic, we only have partial data that are corrupted by possibly high levels of noise. Again, intuition would argue that this would affect the convergence of the method. However, we show below that the rate of convergence is not strongly affected by varying noise. Second, the observations are taken discretely and the timing is difficult to control since this requires a clinic visit. We show that increasing the gap between observations leads to fast convergence to the parameter estimate.

The parameter estimation method that we use here is the direct filter as we discussed above. For the AA model, we use finite difference scheme to discretize the PDE system defined in (1)–(3) and collect observations for the solutions T4 and T8 for the time period from t=0 to t=3. In the numerical experiments in this section, we study the parameter estimation performance in estimating  $\alpha$  and  $\beta$  which represent T8 activation rate and T4 activation rate, respectively. In this work, we assume that all the parameters for the AA model are known (Dobreva *et al.*, 2020, 2015, 2017). Specifically, we use the conclusion in Dobreva *et al.* (2015) to fix  $\alpha=0.08 \mathrm{pg}^{-1}$  and  $\beta=0.8975 \mathrm{pg}^{-1}$  as our 'true' parameters. To generate observational data, we use the true  $\alpha$  and  $\beta$  to simulate the AA model and generate synthetic real state of the model. Then we perturb the real state by some observational noise. We assume that the observational noises  $\{\epsilon_n\}$  are generated by random variables following Gaussian distribution with a given standard deviation  $\sigma$ .

In Fig. 1, we plot the simulated solutions for T4 and T8. The timescale presented here is guided by the convergence of the parameter estimation procedure. The model has been developed to apply for clinically relevant timescales (see Dobreva *et al.*, 2020). However, part of the goal here is to determine how fast the parameter estimation converges—which is related to the number and frequency of observations. Thus, the DA would be unchanged by collecting more observations.

In Fig. 2, we demonstrate the behaviour of our noisy observation of the solution T4 and T8 with noise level  $\sigma = 0.05$ .

#### **Experiment 1: estimating parameters with different sensitivities**

A typical interpretation of parameter sensitivity is that sensitive parameters are important and have a large affect on the output. This means accurate estimates are required for accurate predictions. One might think that this might make it more difficult to estimate the parameter, but we show here that this method converges faster for the more sensitive parameter. This is because the direct filter method adjusts faster for greater discrepancy between the model and the observation.

#### DATA ASSIMILATION OF SYNTHETIC DATA

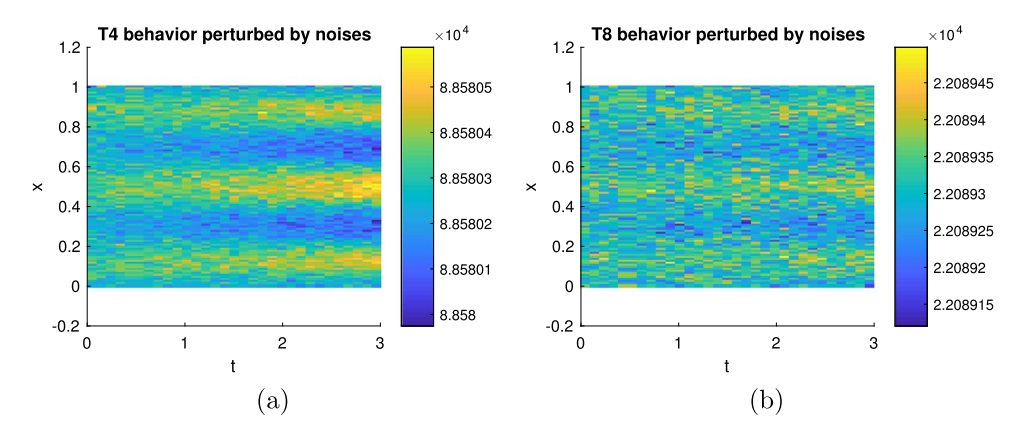


Fig. 2. We simulate the development of the spatial pattern obtained from numerical simulations of (1)–(3) with added noise ( $\sigma = 0.05$ ). Parameter values are given in Table 1. (a) Noise perturbed T4. (b) Noise perturbed T8.

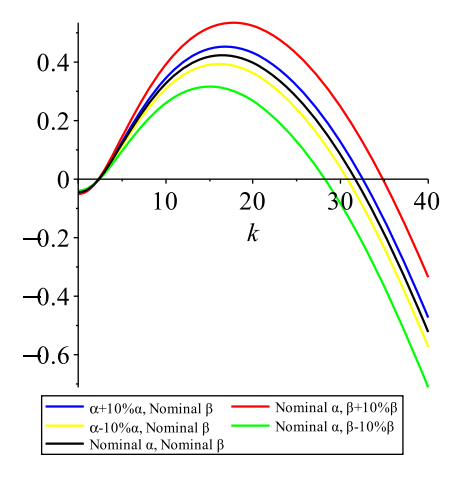


Fig. 3. Impact of 10% change in  $\alpha$  and  $\beta$  on the dispersion relation. We see that varying  $\beta$  leads to quantitatively larger change in the peak of the dispersion curve which is an estimate for the observed pattern frequency.

Figure 3 shows how changes in the parameters  $\alpha$  and  $\beta$  influence the dispersion relation for the PDE model and thereby the pattern arising from IFNg and immune cell dynamics. The dispersion relation, which defines  $\lambda$  in terms of k, indicates the relative growth rate of modes with different spatial frequency. We derive this from classic linear stability analysis of a PDE system by perturbing a stationary solution and analysing the linearized system (Murray, 2007; Segel, 1984). When the dispersion curve is below the k-axis ( $\lambda$  is negative), this corresponds to no pattern (a uniform steady state), i.e. no AA presentation. The peak of the dispersion curve indicates the emergence of a most unstable mode, which means that a pattern arises. The pattern is formed by low and high levels of the immune components, and in the AA context, this means disease development. In Fig. 3, there is 10% variation applied to both parameters and we use this to quantify the sensitivity of the pattern (e.g. the wavelength corresponding to the maximal growth rate). The most basic definition of a sensitivity measure of a QOI with respect to a parameter, p, is  $\frac{\partial (QOI)}{\partial p}$ . We approximate this derivative using the 10% variations and estimate that  $\beta$  is

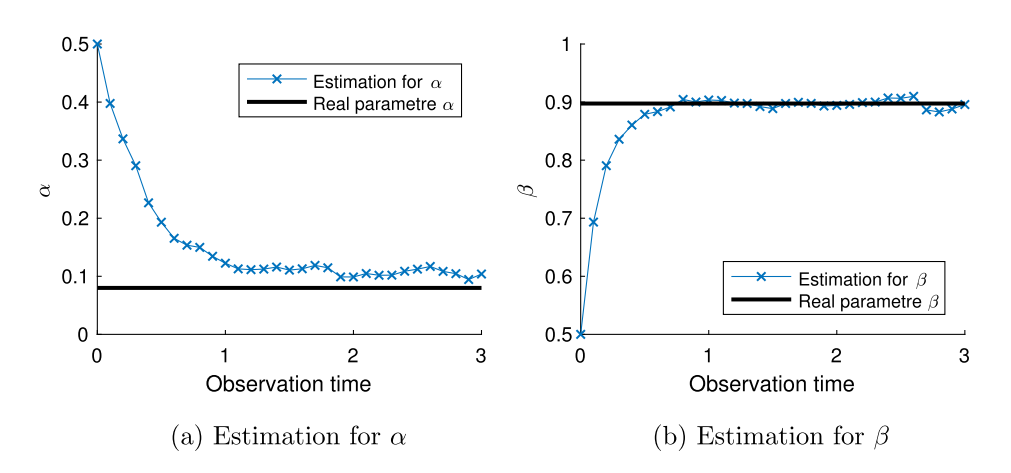


Fig. 4. Parameter estimation for  $\alpha$  and  $\beta$ .

approximately three times more sensitive with respect to the pattern development. Specifically, we find that  $\frac{\partial k_{max}}{\partial \beta} \approx 3.008$  and  $\frac{\partial k_{max}}{\partial \alpha} \approx 1.002$ .

We assume that the standard deviation of the observational noise is  $\sigma = 1$  and collect observational data with a given observational gap  $\Delta t = 0.1$ . Therefore, we have altogether 30 sets of observational data to estimate the parameters.

In Fig. 4, we plot the parameter estimation results for estimating  $\alpha$  and  $\beta$  with respect to the observation time. In Fig. 4(a), we show the estimation for  $\alpha$  and in Fig. 4(b) we show the estimation for  $\beta$ . The black straight line in each subplot is the real invariant parameter and the blue curves marked by crosses show the estimation obtained by using the direct filter method. From this figure, we can see that the direct filter takes about 5 observations to capture an accurate estimation for the parameter  $\beta$  while it takes approximately 10 observations to obtain a relatively accurate estimation for the parameter  $\alpha$ .

Since the above experiment presents the accuracy and effectiveness of our parameter estimation method in processing only one realization of the observational data, in what follows we repeat the above experiments 100 times with different realizations of observational data, which are generated from different random samples in observational noise, to examine the robustness of the direct filter performance. Specifically, we calculate the root mean square errors (RMSEs) in estimating  $\alpha$  and  $\beta$  in the repeated experiments, and the RMSE for the parameter  $\theta$  is defined as

$$RMSEs(n) := \sqrt{\frac{1}{MC} \sum_{i=1}^{MC} \|\tilde{\theta}_n - \theta\|^2},$$
(10)

where  $\tilde{\theta}_n$  is the estimated parameter at observation step n and MC is the number of random samples, which is chosen to be MC = 100 in this experiment.

In Fig. 5, we plot the RMSEs for  $\alpha$  and  $\beta$  estimation over the observation time. The blue curves marked by crosses show the RMSEs in each subplot. We can see from this figure that on average the direct filter takes about 5 observations to capture the true parameter for  $\beta$  and it takes about 10 steps to obtain a good estimation for  $\alpha$ . Therefore, from both the single realization and multi-realization

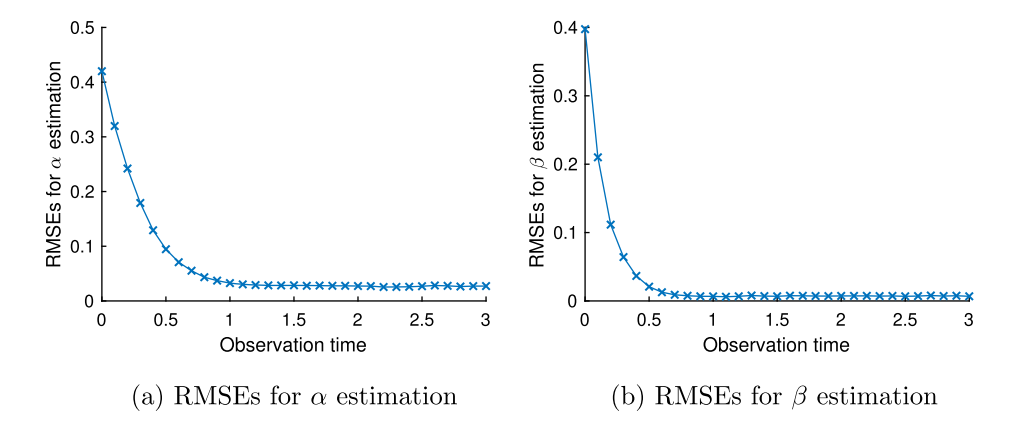


Fig. 5. RMSEs for the parameter estimation.

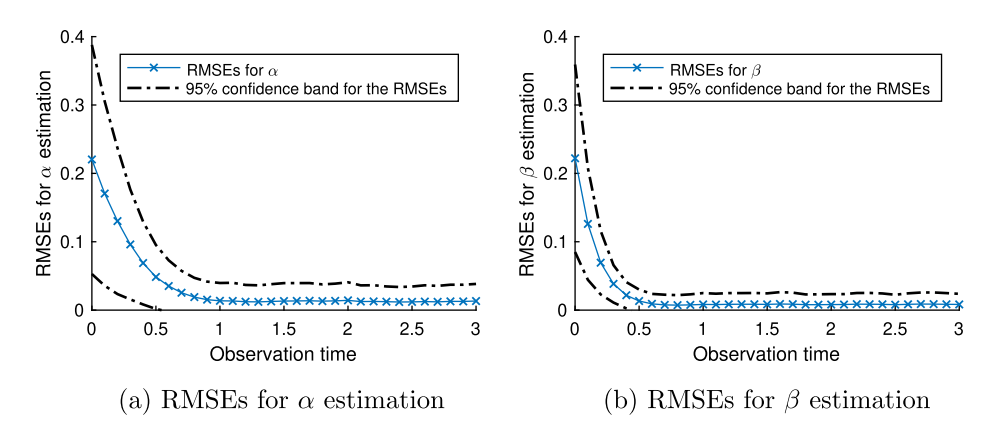


Fig. 6. RMSEs for the parameter estimation for 100 samples within 10% variation of the nominal set with the 95% confidence interval shown.

experiments, we observe that it is faster to capture more sensitive parameter  $\beta$  and the  $\beta$  estimation is more accurate.

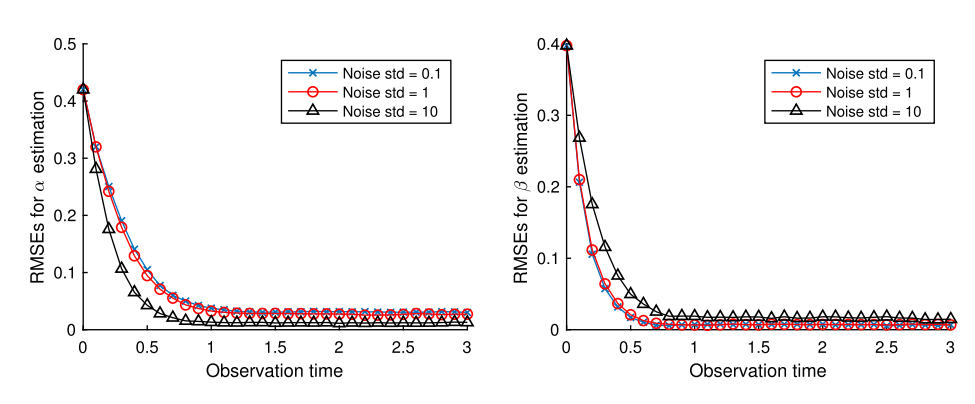
If we also include stochastic variations in the true parameter values, we can explore how much the convergence depends on the region in parameter space that we are exploring. We make no broad claims about convergence throughout all parameter space. We can explore the impact of 10% variations in the true values of  $\alpha$  and  $\beta$ . We do this by selecting 100 random pairs of parameters within 10% of the nominal set and running the data assimilation algorithm. This provides us with samples of the method where we can assign 95% confidence intervals to the RMSE convergence plots (see Fig. 6).

#### **Experiment 2: effects of noise on parameter estimation**

Observations are always contaminated with noise. In observations on the character, extent and spread of AA lesions by clinical inspection and photodocumentation, we expect the noise to be large since these non-invasive and at best semi-quantitative observations are difficult to compare and standardize. Attempts have been made to standardize the severity assessment of AA, e.g. by the Severity of Alopecia Tool (SALT Score Computation) (Bernardis & Castelo-Soccio, 2018; Bernardis *et al.*, 2018; Olsen

N. G. COGAN ET AL.

12



- (a) RMSEs for  $\alpha$  with different observational noise
- (b) RMSEs for  $\beta$  with different observational noise

Fig. 7. RMSEs with different observational noise.

et al., 2018; Solomon, 2015) and by recording and scoring hair loss in defined scalp surface quadrants using the Alopecia Areata Progression Index (AAPI) (Jang et al., 2016). However, there is still no fully satisfactory, universally accepted and widely employed standardized method for accurately quantifying the extent and progression of AA lesions, and even the rigorous application of SALT or AAPI scores generates much observer-to-observer variation and thus considerable noise. One might expect that increasing noise would make it more difficult to estimate the parameters since standard optimization methods attempt to minimize the discrepancy between model and data. The residual will typically be contaminated by the noise. Here we show that this is not the case. Instead, the estimates get better as the noise level increases.

To demonstrate the influence of the observational noise in the parameter estimation, we examine the performance of the direct filter in the parameter estimation with various observational noise. Specifically, we let the standard deviation for the observational noise be  $\sigma = 0.1, 1, 10$ . At time t = 3, the difference in T4 over the simulation interval, i.e.  $\max(T4) - \min(T4)$ , is only 0.4287; the difference in T8 over the simulation interval, i.e.  $\max(T8) - \min(T8)$ , is only 0.1293. This indicates that the direct filter method could provide accurate estimation for the parameters effectively and accurately even when we have inaccurate observations.

In Fig. 7, we plot the RMSEs corresponding to  $\alpha$  estimation and  $\beta$  estimation in subplots (a) and (b), respectively. Although there are some differences in the parameter estimation, our direct filter method is not very sensitive to the level of observational noise. For the  $\beta$  estimation, we can see that we obtain almost the same results by using observational data with noise levels  $\sigma=0.1$  and  $\sigma=1$ . When the observational noise is very large, i.e.  $\sigma=10$ , we observe slower convergence for  $\beta$  estimation with higher RMSEs. On the other hand, we can see from Fig. 7(a) that we actually obtain better estimation for  $\alpha$  when the observational noise is larger. Since  $\alpha$  is not as sensitive a parameter, it is less affected by noise.

**Experiment 3: effect of the gap in observation time on parameter estimation** Our next numerical experiment considers the gap between observations. Intuitively, one might assume that more frequent observations would provide faster convergence to parameter estimates. From a clinical standpoint, this creates difficulty since each observation is gathered by an office visit by a patient, so many observations require many office visits. But again, because the steering used in the direct filter method penalizes

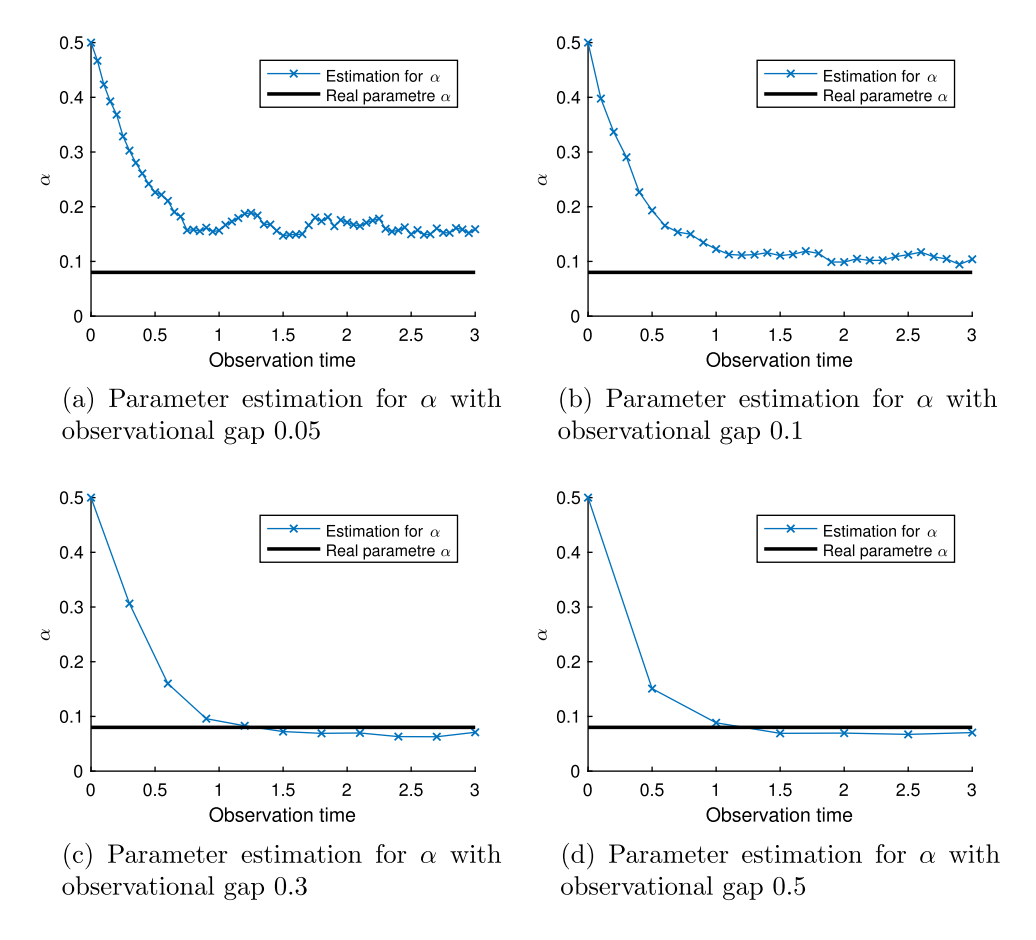


Fig. 8. Parameter estimation for  $\alpha$  with observational gaps 0.05, 0.1, 0.3 and 0.5.

large deviations, rapid observations are not optimal since there is little variation between observations. Instead larger gaps can provide faster convergence.

In what follows, we carry out parameter estimation experiments for fixed standard deviation  $\sigma=1$  in the observational noise. At the same time, we choose the observational gap to be  $\Delta t=0.05, 0.1, 0.3, 0.5$  and process the observational data.

In Figs 8 and 9, we present the parameter estimation performance of the direct filter in estimating parameters  $\alpha$  and  $\beta$ , respectively, with observational gaps  $\Delta t = 0.05, 0.1, 0.3, 0.5$  (in subplots (a), (b), (c) and (d), respectively). In each subplot, the black straight line shows the invariant true parameter and the blue curve marked by crosses presents the estimation for the parameter. From Fig. 8, we observe that the direct filter provides smaller errors for the parameter estimation if we use larger observational gaps. On the other hand, if we take very frequent observations, it does not converge to the true parameter well. In our data assimilation approach for estimating parameters in the AA model, we use a stochastic dynamical system to model the target parameters and use observations on states of the AA model as data to adjust our estimates for the parameters. When incorporating too frequent observations, the data are more frequently contaminated by noise since the states of the AA model are relatively fixed and the

14

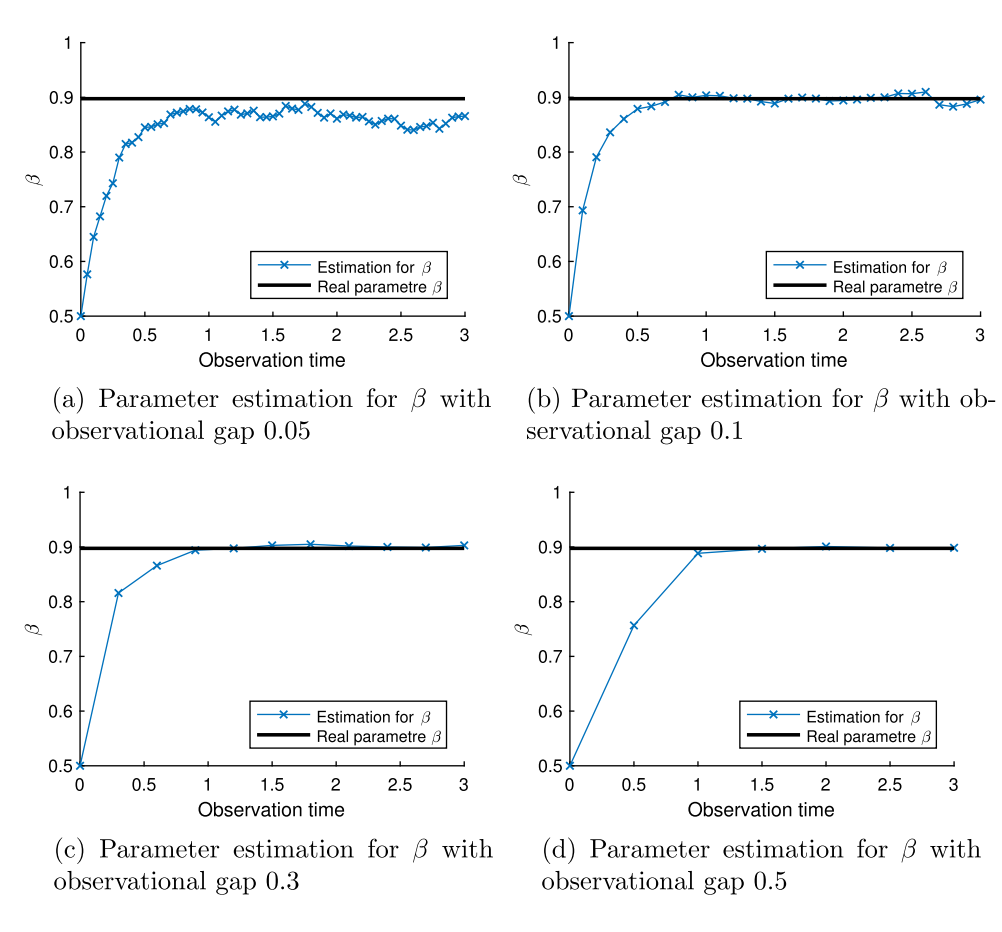


Fig. 9. Parameter estimation for  $\beta$  with observational gaps 0.05, 0.1, 0.3 and 0.5.

level of noise remains the same. Therefore, over-sampling observed data does not provide us enough effective information to generate narrow likelihoods to derive more accurate estimates. While the model propagation does not provide sufficient model information, too frequent observations may not collect enough useful information. From Fig. 9, we observe similar behaviour as we can see in Fig. 8.

To provide more evidence for our discussion on the data collection frequency, we repeat the above experiment 100 times with different realizations for the random variables and calculate the RMSEs for each parameter estimation with observational gaps  $\Delta t = 0.05, 0.1, 0.3, 0.5$ . The corresponding RMSEs are presented in Figs 10 and 11. In Fig. 10, we plot the RMSEs for the  $\alpha$  estimations, and in Figure 11, we plot the  $\beta$  estimations. From the RMSEs, we can see that by repeating the parameter estimation experiments with different random samples of the observational data, we obtain the same behaviour of the parameter estimation.

#### **Experiment 4: estimation for various choices of parameters**

In our final experiment, we examine the performance of our parameter estimation method by estimating various parameters. To proceed, we select parameters  $\alpha_i$  and  $\beta_i$ ,  $i=1,2,\cdots,20$ , which are randomly generated as  $\alpha_i \sim 0.3 + N(0,\epsilon^2)$  and  $\beta_i \sim 0.7 + N(0,\epsilon^2)$  for a pre-chosen parameter

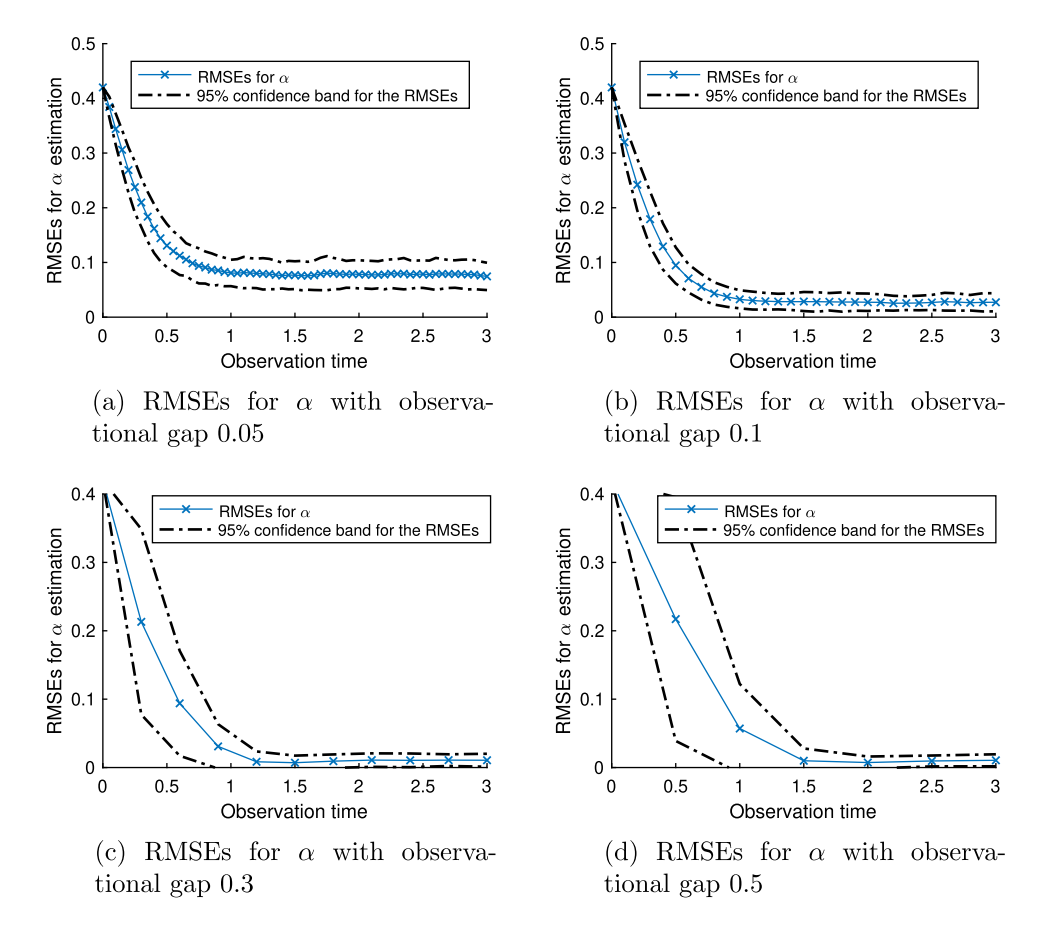


Fig. 10. RMSEs for  $\alpha$  with observational gaps  $\Delta t = 0.05, 0.1, 0.3, 0.5$ .

noise level  $\epsilon = 0.075$ . Then, we carry out our parameter estimation method to estimate each pair of parameters  $(\alpha_i, \beta_i)$ . In Figure 12,

we present the estimation performance for our various choices of parameters, where the colourful crosses represent real parameters and the colourful circles give our estimated parameters corresponding to true parameters. From this figure, we can see that the parameter estimation method accurately captured all 20 randomly selected true parameter values with very small errors.

To further demonstrate the accuracy of our method over the observation period, we plot the RMSEs, which combine errors across all the randomly selected parameters, in Fig. 13.

We can see from this figure that the RMSEs decrease quickly and could reach very low errors, which indicates the robust effectiveness of our method in estimating various choices of parameters.

#### 5. Discussion

One goal of personalized medicine is incorporating observational data into treatment plans. Observations are almost always incomplete and contaminated by noise that enters the system through the obser-

16

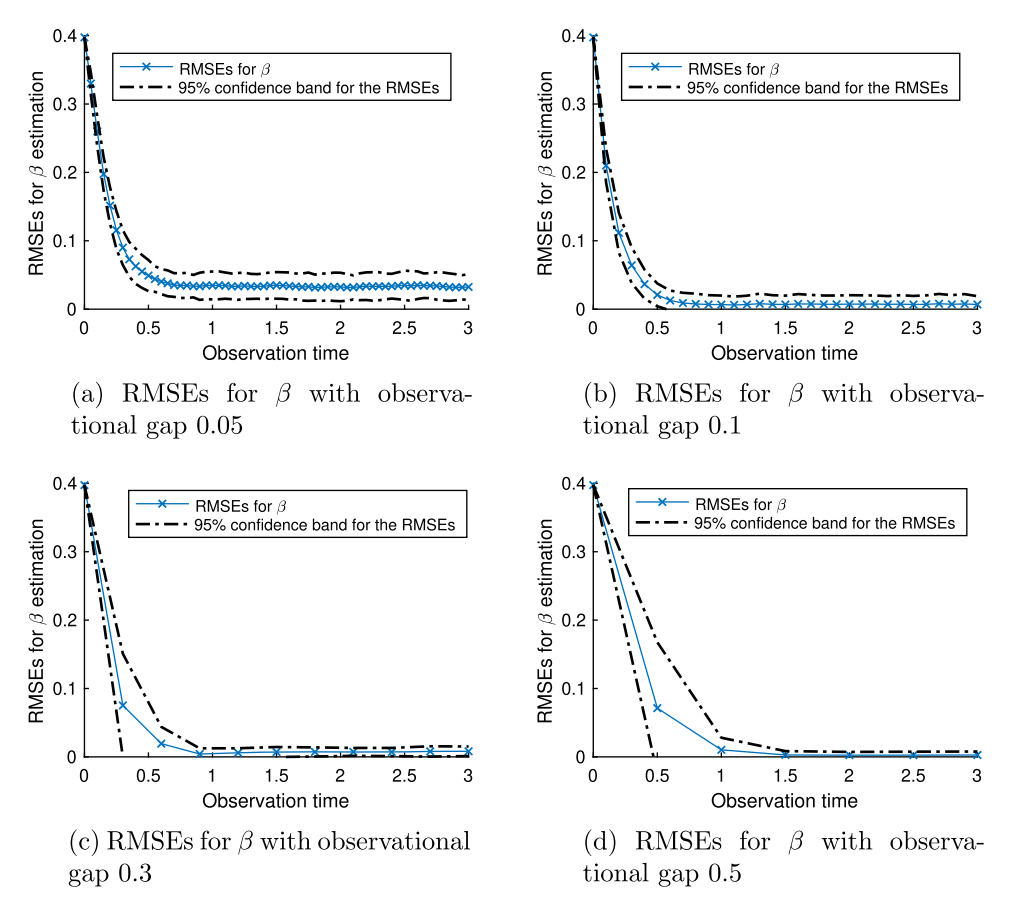


Fig. 11. RMSEs for  $\beta$  with observational gaps  $\Delta t = 0.05, 0.1, 0.3, 0.5$ .

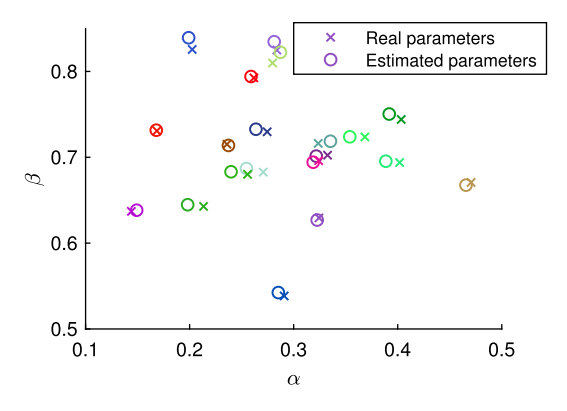


Fig. 12. Estimation performance for various choices of parameters.

vational methods and inherent variability within a patient. Data assimilation is a broad methodology used to incorporate observations into mathematical models to 'steer' the model predictions. There is a

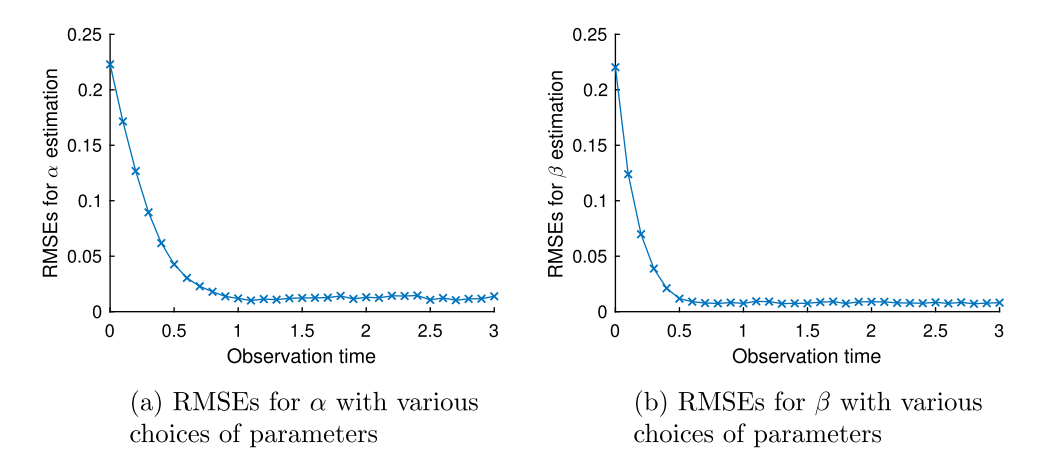


Fig. 13. RMSEs with various choices of parameters.

need for methods that can incorporate incomplete and uncertain data into accurate mathematical models designed to address treatments.

This manuscript demonstrates a recently developed DA method that uses optimal filters to estimate key parameters that describe patterns observed in a model of AA. We use synthetic data to demonstrate several non-intuitive aspects of this method in terms of biologically relevant modelling concepts. The model has been shown to be consistent with the immune privilege collapse explanation of the progression of AA. The spatial and temporal scale of the developing pattern, which is a hallmark of the disease, is a key prediction from analysing the model via the immune cell estimates. We use this output, coupled with noisy, synthetic data to demonstrate some key features of our method. We show that this method is accurate even with noisy data, infrequent and partial observations. The method exploits higher variations to guide the parameter estimation so that more less frequent observations and parameters that are more sensitive with respect to the pattern output provide more information/guidance. We do not claim that our method of parameter estimation is insensitive to these variations for all models; however, we are able to conclude that the inverse method provides a unique insight into the disease process. These results are counter-intuitive since it is commonly assumed that sensitive parameters are the most difficult to estimate and require complete data. This leads us to believe that our methodology may provide a route to personalized medicine that can adjust treatments during the progression.

#### Acknowledgements

AD was supported by National Science Foundation grant RTG/DMS-1246991. RP was supported by NIHR Manchester Biomedical Research Centre, "Inflammatory Hair Diseases" Programme. FB was supported by NSF Award #1720222.

#### REFERENCES

Andrieu, C., Doucet, A. & Holenstein, R. (2010) Particle Markov chain Monte Carlo methods. *J. R. Statist. Soc. B*, **72**, 269–342.

AL-NUAIMI, Y., GOODFELLOW, M., PAUS, R. & BAIER, G. (2012) A prototypic mathematical model of the human hair cycle. *J. Theor. Biol.*, **310**, 143–159.

AQ7

AQ8

- ARCHIBALD, R., BAO, F. & Tu, X. (2019) A direct filter method for parameter estimation. *J. Comput. Phys.*, **398**, 108871.
- Dobreva, A., Paus, R. & Cogan, N. G. (2020) Toward predicting the spatio-temporal dynamics of alopecia areata lesions using partial differential equation analysis. *Bull. Math. Biol.*, **82**, 1–32.
- Bernardis, E. & Castelo-Soccio, L. (2018) Quantifying alopecia areata via texture analysis to automate the salt score computation. *J. Investig. Dermatol. Symp. Proc.*, **19**, S34–S40.
- Bernardis, E., Nukpezah, J., Li, P., Christensen, T. & Castelo-Soccio, L. (2018) Pediatric severity of alopecia tool. *Pediatr. Dermatol.*, **35**, e68–e69.
- BAO, F. & MAROULAS, V. (2017) Adaptive meshfree backward SDE filter. SIAM J. Sci. Comput, 39, A2664–A2683.
  BAO, F., CAO, Y. & HAN, X. (2021) Forward backward doubly stochastic differential equations and optimal filtering of diffusion processes. Commun. Math. Sci. arxiv: 1509.06352.
- BAO, F., CAO, Y. & CHI, H. (2019) Adjoint forward backward stochastic differential equations driven by jump diffusion processes and its application to nonlinear filtering problems. *Int. J. Uncertain. Quantif.*, **9**, 143–159.
- BERTOLINI, M., ZILIO, F., ROSSI, A., KLEDITZSCH, P., EMELIANOV, V. E., GILHAR, A., KEREN, A., MEYER, K. C., WANG, E., FUNK, W., et al. (2014) Abnormal interactions between perifollicular mast cells and cd8+ t-cells may contribute to the pathogenesis of alopecia areata. *PLoS One*, **9**, e94260.
- DEL MORAL, P., KURTZMANN, A. & TUGAUT, J. (2018) On the stability and the concentration of extended Kalman–Bucy filters. *Electron. J. Probab.*, **23**, 30.
- Dobreva, A., Paus, R. & Cogan, N. G. (2015) Mathematical model for alopecia areata. J. Theor. Biol., 380, 332–345.
- Dobreva, A., Paus, R. & Cogan, N. G. (2017) Analysing the dynamics of a model for alopecia areata as an autoimmune disorder of hair follicle cycling. *Math. Med. Biol.*, **35**, 387–407.
- WANG, E. H. C., SALLEE, B. N., TEJEDA, C. I. & CHRISTIANO, A. M. (2018) Jak inhibitors for treatment of alopecia areata. *J. Invest. Dermatol.*, **138**, 1911–1916.
- AQ9 EVENSEN, G. (2006) Data Assimilation: The Ensemble Kalman Filter. Springer.
  - EVENSEN, G. (2009) The ensemble Kalman filter for combined state and parameter estimation: Monte Carlo techniques for data assimilation in large systems. *IEEE Control Syst. Mag.*, **29**, 83–104.
  - GILHAR, A., ETZIONI, A. & PAUS, R. (2012) Medical progress: alopecia areata. N. Engl. J. Med., 366, 1515-1525.
  - GILHAR, A., KEREN, A., SHEMER, A., ULLMANN, Y. & PAUS, R. (2013) Blocking potassium channels (kv1. 3): a new treatment option for alopecia areata? *J. Invest. Dermatol.*, **133**, 2088.
  - GORDON, N. J., SALMOND, D. J. & SMITH, A. F. M. (1993) Novel approach to nonlinear/non-Gaussian Bayesian state estimation. *IEE Proc. F*, **140**, 107–113.
  - Pratt, C. H., King Jr, L. E., Messenger, A. G., Christiano, A. M. & Sundberg, J. P. (2017) Alopecia areata. *Nat. Rev. Dis. Primers*, **3**, 17011.
  - ITO, T., ITO, N., SAATOFF, M., HASHIZUME, H., FUKAMIZU, H., NICKOLOFF, B. J., TAKIGAWA, M. & PAUS, R. (2008) Maintenance of hair follicle immune privilege is linked to prevention of nk cell attack. *J. Invest. Dermatol.*, **128**, 1196–1206.
  - IKEDA, T. (1965) A new classification of alopecia areata. Dermatologica, 131, 421–445.
  - KANG, K., MAROULAS, V., SCHIZAS, I. & BAO, F. (2018) Improved distributed particle filters for tracking in a wireless sensor network. *Comput. Statist. Data Anal.*, 117, 90–108.
  - STRAZZULLA, L. C., WANG, E. H. C., AVILA, L., SICCO, K. L., BRINSTER, N., CHRISTIANO, A. M & SHAPIRO, J. (2018) Alopecia areata: disease characteristics, clinical evaluation, and new perspectives on pathogenesis. *J. Am. Acad. Dermatol.*, **78**, 1–12.
  - Petukhova, L., Duvic, M., Hordinsky, M., Norris, D., Price, V., Shimomura, Y., Kim, H., Singh, P., Lee, A., Chen, W. V., et al. (2010) Genome-wide association study in alopecia areata implicates both innate and adaptive immunity. *Nature*, **466**, 113.
  - PITT, M. K. & SHEPHARD, N. (1999) Filtering via simulation: auxiliary particle filters. *J. Amer. Statist. Assoc.*, **94**, 590–599.
  - MURRAY, J. D. (2007) Mathematical Biology: I/II. An Introduction, vol. 17. Springer Science & Business Media.

- MORZFELD, M., Tu, X., ATKINS, E. & CHORIN, A. J. (2012) A random map implementation of implicit filters. *J. Comput. Phys.*, **231**, 2049–2066.
- Olsen, E. A., Roberts, J., Sperling, L., Tosti, A., Shapiro, J., McMichael, A., Bergfeld, W., Callender, V., Mirmirani, P., Washenik, K., et al. (2018) Objective outcome measures: collecting meaningful data on alopecia areata. *J. Am. Acad. Dermatol.*, **79**, 470–478.
- Paus, R., Theoharides, T. C. & Arck, P. C. (2006) Neuroimmunoendocrine circuitry of the 'brain-skin connection'. *Trends Immunol.*, **27**, 32–39.
- PHAN, K. & SEBARATNAM, D. F. (2019) Jak inhibitors for alopecia areata: a systematic review and meta-analysis. J. Eur. Acad. Dermatol. Venereol., 33, 850–856.
- SEGEL, L. A. (1984) Modeling Dynamic Phenomena in Molecular and Cellular Biology. Cambridge University Press.
- SOLOMON, J. A. (2015) Development of uniform protocol for alopecia areata clinical trials. *J. Investig. Dermatol. Symp. Proc.*, **17**, 63–66.
- VAN LEEUWEN, P. J. (2010) Nonlinear data assimilation in geosciences: an extremely efficient particle filter. *Q. J. Roy. Meteor. Soc.*, **136**, 1991–1999.
- Tong, X. T., Majda, A. J. & Kelly, D. (2016) Nonlinear stability and ergodicity of ensemble based Kalman filters. *Nonlinearity*, **29**, 657–691.
- Jang, Y. H., Moon, S. Y., Lee, W. J., Lee, S. J., Lee, W. K., Park, B. C., Kim, H., et al. (2016) Alopecia areata progression index, a scoring system for evaluating overall hair loss activity in alopecia areata patients with pigmented hair: a development and reliability assessment. *Dermatology*, **232**, 143–149.
- Zakai, M. (1969) On the optimal filtering of diffusion processes. *Z. Wahrscheinlichkeitstheorie und Verw. Gebiete*, **11**, 230–243.